Sliding-Mode Control of Quantum Series-Parallel Resonant Converters via Input–Output Linearization

Miguel Castilla, Luis García de Vicuña, Josep María Guerrero, José Matas, and Jaume Miret, *Member, IEEE*

Abstract—**The purpose of this paper is to explore the problem of designing proper sliding-mode controllers to regulate the output voltage of the dc-to-dc quantum series-parallel resonant converter. A control-oriented dynamic model, which appropriately describes the large-signal behavior of the power circuit by average state variables, is first developed. Using input–output feedback linearization, a control design methodology is then presented, which leads to a family of sliding surfaces that make the output voltage behave following a particular large-signal linear dynamics. Among these surfaces, the final configuration is selected taking into account control circuit simplicity as the basic premise. Besides exhibiting the absence of output-voltage errors in steady state, the control solution leads to robust operation with respect to parameter variations and external disturbances. Simulations and experimental results are reported to validate the expected features of the proposed control solution.**

Index Terms—**Feedback linearization, quantum modulation, resonant converter, sliding-mode control.**

I. INTRODUCTION

THE control of resonant power converters has been widely investigated in the literature [1]–[8]. Although the most popular are frequency and phase control, switching losses and electromagnetic interference (EMI) noise are strongly reduced using amplitude modulation by means of a new time-domain operation scheme named quantum-mode control [5]–[8]. To implement this switching technique, sliding-mode control seems to be a good choice due to its excellent properties, such as robustness against both system parameter variations and large-signal external disturbances [9], [10]. The application of this control technique to quantum resonant converters, however, has only been examined in a small number of studies that basically involve the control design of the series-loaded and parallel-loaded topologies [11], [12].

The purpose of this paper is to explore the problem of designing proper sliding-mode controllers to regulate the output voltage of the dc-to-dc quantum series-parallel resonant converter (QSPRC). Besides the good steady-state accuracy the system exhibits, we are especially interested in the synthesis of sliding surfaces that makes the output voltage of the QSPRC behave following a particularly large-signal linear dynamics. This control objective allows the designer to use traditional (linear) control techniques to establish suitable linear dynamics that meets the time-domain converter specifications (maximum settling time, overshoot, etc.).

The control design begins with the development of a control-oriented dynamic model for the open-loop QSPRC. The averaging method reported in [13], among other similar existing techniques [14], [15], is selected to derive the model because the time-varying average variables include the amplitudes and phase angles of resonant state variables, which results in a simpler and easy-to-use dynamic model. Although practical considerations are used in the model derivation (such as the fact that resonant waveforms evolve quickly when compared with output filter variables), the large-signal operation of the QSPRC is preserved as no small-signal approximations are considered. In addition, no assumptions are made to reduce the order of the nonlinear dynamic model; consequently, the performance of the closed-loop power system can be correctly tested.

Next, we consider the use of feedback linearization to design the sliding-mode controller for the QSPRC. Feedback linearization techniques have been successfully used in the control design of conventional (hard switching) dc-to-dc conversion cells [16]–[19]. The main goal of these approaches is to transform the converter bilinear model into a fully linear system, using exact state transformations and feedback (again no small-signal approximations are considered) [20]. However, the application of these interesting techniques has not been widely expanded nowadays, probably because full linearizing control loops require a complex and expensive practical implementation.

As an alternative, and starting from input–output feedback linearization (a partial linearizing approach) [20], this paper presents a design methodology leading to a family of sliding surfaces that force the output voltage of the QSPRC to follow desired linear dynamics. Among these surfaces, the final configuration is selected taking into account control circuit simplicity as the basic premise. Besides exhibiting the absence of output-voltage errors in steady state, the control solution leads to robust operation with respect to parameter variations and external disturbances (in the input voltage and/or in the load). All these features will be evidenced in the following sections.

The effectiveness of the control solution is established by the stability analysis of the closed-loop system dynamics. The analysis yields a set of design restrictions in terms of the converter components and the parameters of the desired output-voltage dynamics. In addition, numerical simulations and experimental results are reported, confirming the validity of the theoretical contributions: 1) the control-oriented dynamic model
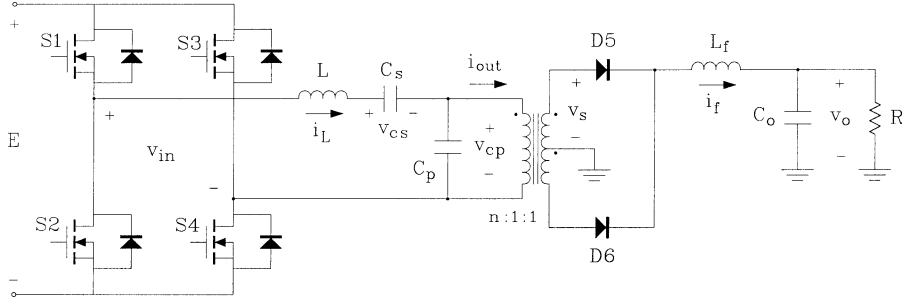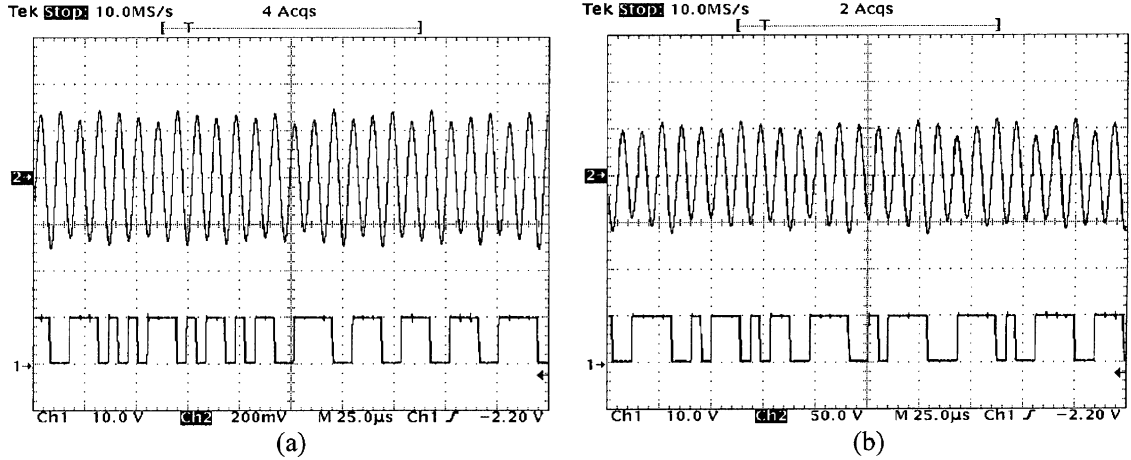
Fig. 1.   Basic topology of the QSPRC.

TABLE I
CHARACTERISTICS OF OPERATIONAL MODES

operation	i_L	S1	S2	S3	S4	v_{in}	P_{input}	v_{cp}	D5	D6	i_{out}	P_{output}
energizing	>0	on	off	off	on	E	$E \cdot i_L > 0$	>0	on	off	i_f / n	$v_{cp} \cdot i_f / n > 0$
	<0	off	on	on	off	-E	$- E \cdot i_L > 0$	<0	off	on	$-i_f / n$	$-v_{cp} \cdot i_f / n > 0$
de-energizing	>0	off	on	off	on	0	0	>0	on	off	i_f / n	$v_{cp} \cdot i_f / n > 0$
	<0	off	on	off	on	0	0	<0	off	on	$-i_f / n$	$-v_{cp} \cdot i_f / n > 0$

Fig. 2.   Typical quantum waveforms. (a) Resonant inductor current (2 A/div). (b) Transformer voltage v_s (50 V/div). Bottom: control signal $u(kT)$ (10 V/div).

of the QSPRC; 2) the design methodology of sliding-mode control schemes; and 3) the proposed control solution.

II. OPERATION PRINCIPLE OF THE QSPRC

The power circuit of the QSPRC is shown in Fig. 1. It consists of a third-order resonant network that includes a high-frequency transformer, excited by a full-bridge inverter and loaded by a rectifier and a low-pass filter.

In the QSPRC, the energy flow between the input source and the load is controlled by two different modes of operation. In the energizing mode (EM), the pair of switches S1-S4 and S2-S3 are switching on and off at resonant frequency, thus transferring energy toward the resonant tank at a maximum rate (the input power to the resonant circuit $P_{\text{input}} = v_{in} \cdot i_L$ is always positive; see Table I). In the de-energizing mode (DM), switches S2 and S4 are constantly in the on state, forcing the input power flowing toward the resonant circuit to be zero. In both modes of operation, the output power of the resonant tank $P_{\text{output}} = v_{cp} \cdot i_{out}$ is always positive, thus continuously supplying part of its energy to the load (see also Table I).

This principle of operation results in sinusoidal resonant waveforms with amplitude modulation. The peak values of these waveforms are increased in EM and decreased in DM. Typical waveforms for a nonperiodic sequence of control modes are shown in Fig. 2. Note how the operational modes present discrete time duration, which coincides with an integer number of half resonant periods.

III. CONTROL-ORIENTED DYNAMIC MODEL

The first problem addressed in this paper is the development of an appropriate dynamic description of the isolated QSPRC converter valid for the design of a nonlinear variable-structure controller.
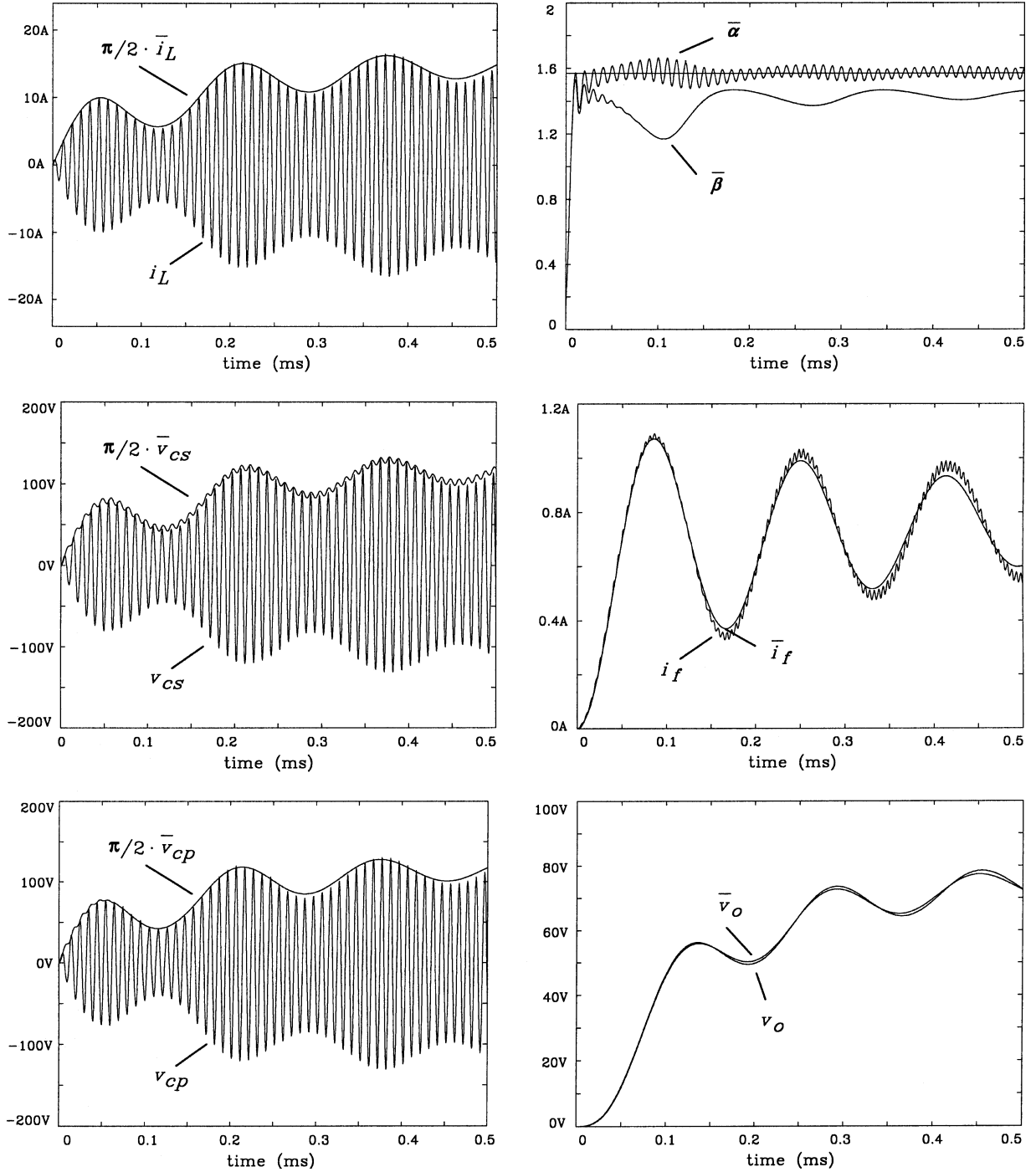
Fig. 3. Waveform comparison of the QSPRC converter with its averaged model.

A. State-Space Model

The power stage of the QSPRC, shown in Fig. 1, can be represented by the following set of differential state equations:

$$\frac{di_L}{dt} = \frac{1}{L} \cdot [u \cdot E \cdot \text{sgn}(i_L) - v_{cs} - v_{cp}] \tag{1}$$

$$\frac{dv_{cs}}{dt} = \frac{1}{C_s} \cdot i_L \tag{2}$$

$$\frac{dv_{cp}}{dt} = \frac{1}{C_p} \cdot \left[i_L - \frac{i_f}{n} \cdot \text{sgn}(v_{cp}) \right] \tag{3}$$

$$\frac{di_f}{dt} = \frac{1}{L_f} \cdot \left[\frac{\text{abs}(v_{cp})}{n} - v_o \right] \tag{4}$$

$$\frac{dv_o}{dt} = \frac{1}{C_o} \cdot \left[i_f - \frac{v_o}{R} \right] \tag{5}$$

where i_L, v_{cs}, and v_{cp} are the resonant state variables (denoting inductor current, series capacitor voltage, and parallel capacitor voltage) and i_f, v_o the output filter state variables (being inductor current and capacitor voltage). The control input u is a discrete-time variable which shows the selected mode of operation: $u = 1$ corresponds to EM and $u = 0$ to DM.
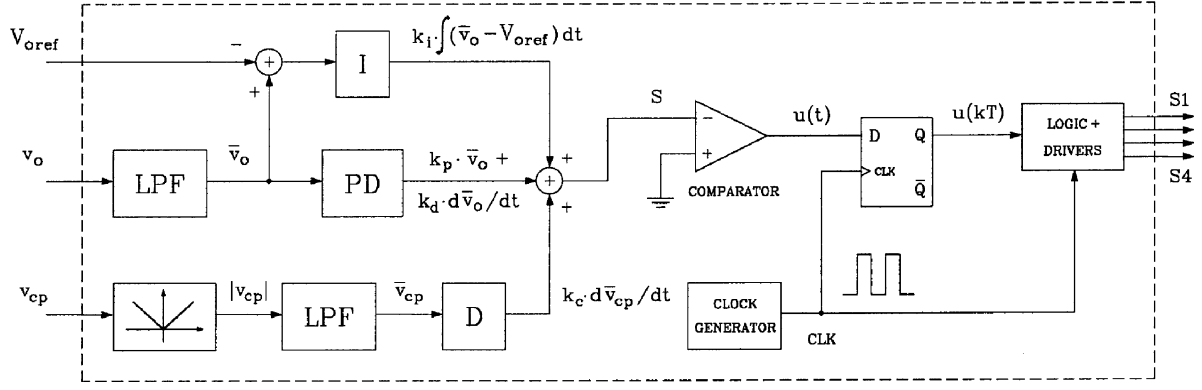
Fig. 4. Diagram of the proposed sliding-mode controller.

TABLE II
NOMINAL VALUES

Power circuit components
$E = 12\,V$, $L = 50\,\mu H$, $C_s = C_p = 100\,nF$
$n = 1$, $L_f = 2\,mH$, $C_o = 2\,\mu F$, $R = 100\,\Omega$
Control parameters
$V_{oref} = 30\,V$, $k_c = 120\,nF$, $k_p = 0.042\,\Omega^{-1}$
$k_i = 50\,(\Omega \cdot s)^{-1}$, $k_d = 10.4\,\mu F$

Fig. 5. Stability region in the $k_p - k_i$ plane.

Fig. 6. Loci of external dynamics eigenvalues varying k_i inside of the stable region.

For the sake of simplicity, no parasitic effects (such as those involving the switches, the inductances, the capacitors, and the transformer) are considered. The error caused by this simplification is indeed absorbed by the controller, as the experimental results show (see Section V).

The high-frequency discontinuities associated with (1)–(5) make the state-space model not directly useful for control design purposes. In the following sections, a set of assumptions is considered in order to derive a control-oriented dynamic model.

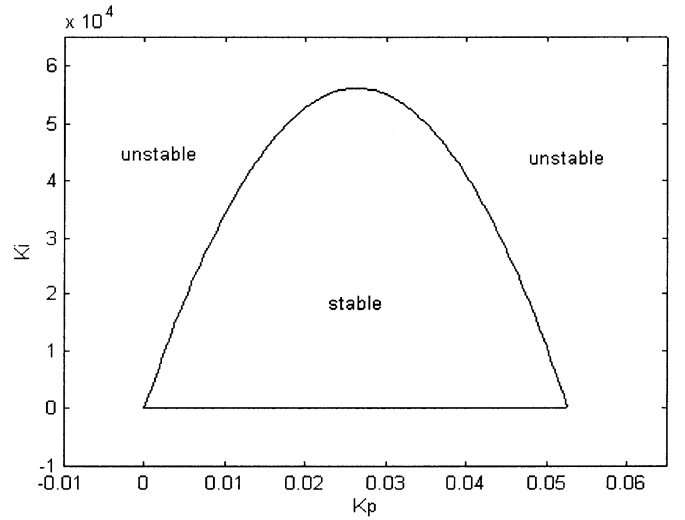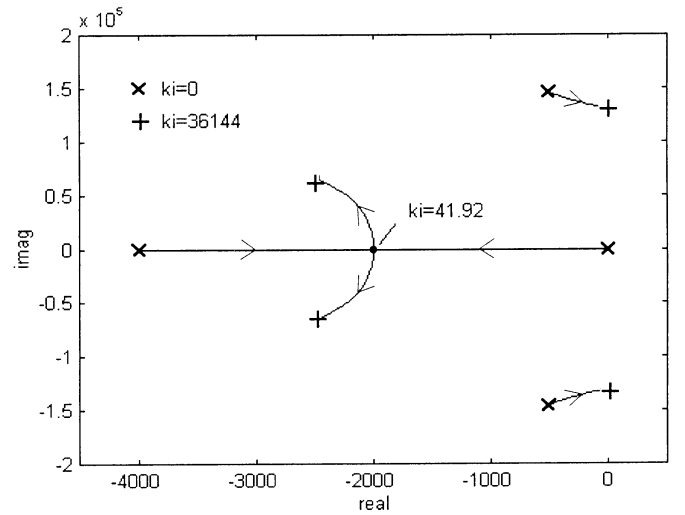### B. Nominal Solution of the Resonant State Variables

Based on the standard practice in resonant circuit design, the resonant state variables are assumed to be purely sinusoidal signals with time-varying amplitudes and phases, which evolve slowly when compared with the switching frequency [13]

$$i_L = I_L \cdot \sin \omega_r t \tag{6}$$

$$v_{cs} = V_{cs} \cdot \sin(\omega_r t - \alpha) \tag{7}$$

$$v_{cp} = V_{cp} \cdot \sin(\omega_r t - \beta). \tag{8}$$

Notice that the quantum operation drives the state variables at exactly the resonant frequency ω_r and forces the phase angle associated with the resonant inductor current to be always zero

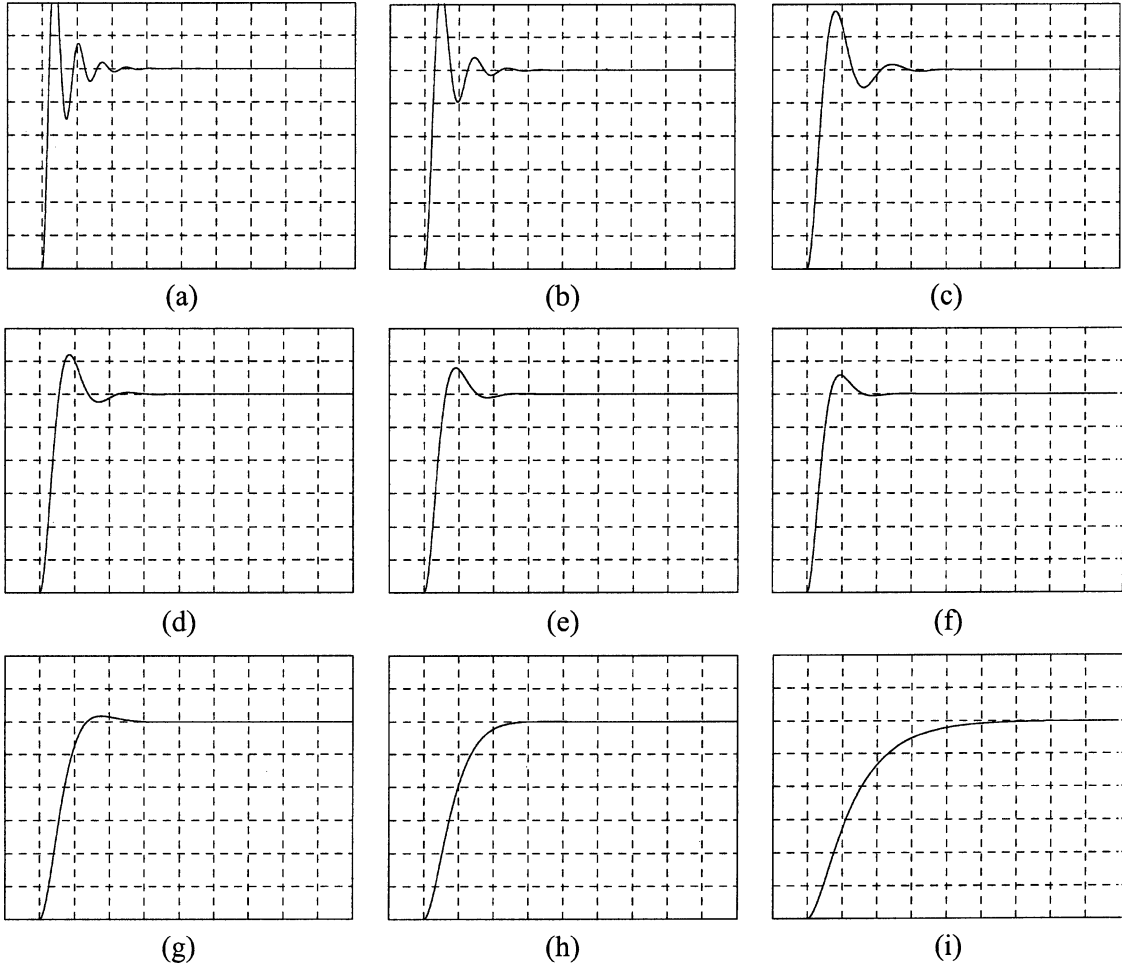(the input voltage of the resonant circuit v_{in} is defined as the origin of the phase angles).

Fig. 7. Simulation results of the output-voltage startup for the different values of k_i: (a) 920, (b) 535, (c) 325, (d) 200, (e) 145, (f) 120, (g) 75, (h) 50, and (i) 30. Output voltage: 5 V/div. Time: 1 ms/div.

The angular resonant frequency can be calculated using fundamental frequency techniques [21], resulting in

$$\left(\frac{\omega_r}{\omega_o}\right)^2 = \frac{(1+A)\cdot B - 1 + \sqrt{((1+A)\cdot B - 1)^2 + 4AB}}{2\cdot(1+A)\cdot B} \tag{9}$$

with $\omega_o = 1/\sqrt{LC}$, $C = C_s \cdot C_p/(C_s + C_p)$, $A = C_p/C_s$, $B = (1+A)\cdot Q^2$, $Q = n^2 R/Z_o$, and $Z_o = \sqrt{L/C}$.

C. Averaged Large-Signal Model

Taking into account that the time scale of the output filter is much longer than the resonant tank, the ripple appearing in the output filter state variables is negligible and, thus, i_f and v_o can be approximated accurately by means of their time-varying average values $\bar{i}_f$ and $\bar{v}_o$. Then, averaging (4) and (5) over one switching period yields

$$\frac{d\bar{i}_f}{dt} = \frac{1}{L_f}\cdot\left[\frac{\bar{v}_{cp}}{n} - \bar{v}_o\right] \tag{10}$$

$$\frac{d\bar{v}_o}{dt} = \frac{1}{C_o}\cdot\left[\bar{i}_f - \frac{\bar{v}_o}{R}\right] \tag{11}$$

with $\bar{v}_{cp}$ the local average value of $abs(v_{cp})$, that is, $\bar{v}_{cp} = (2/\pi)\cdot V_{cp}$.

Similarly, the average variables $\bar{i}_L$ and $\bar{v}_{cs}$ can be defined as the local average values of $abs(i_L)$ and $abs(v_{cs})$, respectively. The phase angles $\bar{\alpha}$ and $\bar{\beta}$ are the time-varying average values of α and β. The averaged model for these variables can be obtained by first inserting the nominal solution (6)–(8) into the resonant equations (1)–(3) and substituting the nonlinear elements by their fundamental harmonic components; and second, by imposing harmonic balance on the coefficients of the linear combination of functions $\sin\omega_r t$ and $\cos\omega_r t$ [13], resulting in

$$\frac{d\bar{i}_L}{dt} = \frac{1}{L_{\text{eq}}}\cdot\left[u\cdot E - \frac{Z_o\cdot\omega_o}{n\cdot(1+A)\cdot\omega_r}\cdot\bar{i}_f\cdot\sin\bar{\beta}\right] \tag{12}$$

$$\frac{d\bar{v}_{cs}}{dt} = \frac{AZ_o\omega_o}{1+A}\cdot\bar{i}_L\cdot\cos\bar{\alpha} \tag{13}$$

$$\frac{d\bar{v}_{cp}}{dt} = \frac{1}{C_{\text{eq}}}\cdot\left[\frac{\pi^2}{8}\cdot\bar{i}_L\cdot\cos\bar{\beta} - \frac{\bar{i}_f}{n}\right] \tag{14}$$

$$\frac{d\bar{\alpha}}{dt} = \omega_o\cdot\left[\frac{\omega_r}{\omega_o} - \frac{AZ_o}{1+A}\cdot\frac{\bar{i}_L\cdot\sin\bar{\alpha}}{\bar{v}_{cs}}\right] \tag{15}$$

$$\frac{d\bar{\beta}}{dt} = \omega_o\cdot\left[\frac{\omega_r}{\omega_o} - \frac{Z_o}{1+A}\cdot\frac{\bar{i}_L\cdot\sin\bar{\beta}}{\bar{v}_{cp}}\right] \tag{16}$$

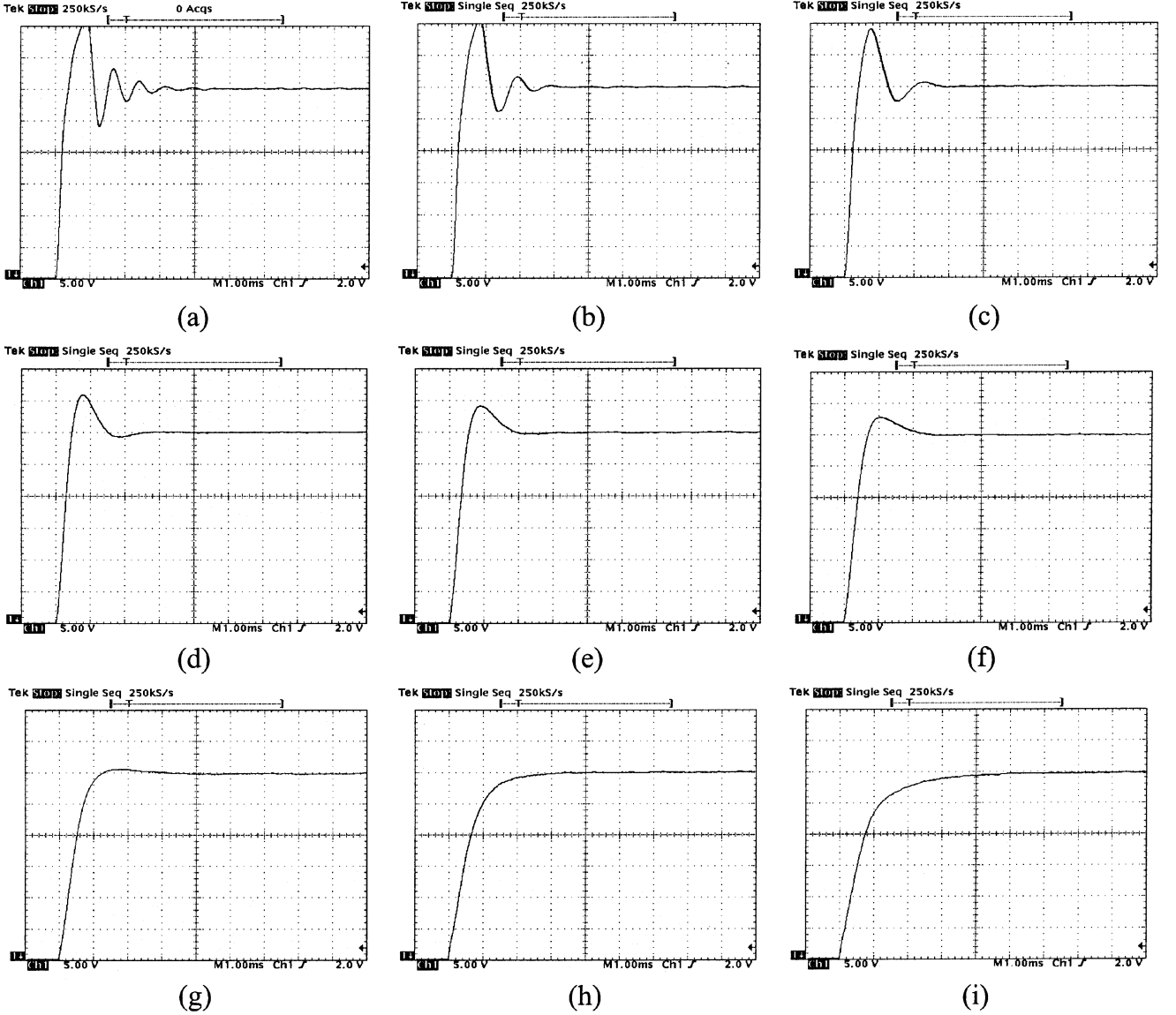with $L_{\text{eq}} = \pi^2\cdot L/4$ and $C_{\text{eq}} = \pi^2\cdot(1+A)\cdot C/8$.

Fig. 8. Experimental output-voltage startup for the different values of k_i: (a) 920, (b) 535, (c) 325, (d) 200, (e) 145, (f) 120, (g) 75, (h) 50, and (i) 30. Output voltage: 5 V/div. Time: 1 ms/div.

Equations (10)–(16) form a seventh-order large-signal model involving the average variables $\bar{i}_L$, $\bar{v}_{cs}$, $\bar{v}_{cp}$, $\bar{\alpha}$, $\bar{\beta}$, $\bar{i}_f$, and $\bar{v}_o$. A comparison of the waveforms generated by this model and the state-space model when the converter operates in energizing mode ($u = 1$) is depicted in Fig. 3. The power circuit components used in the simulation are shown in Table II. As the figure shows, the correlation between the two models is very good.

IV. CONTROL DESIGN BASED ON INPUT–OUTPUT LINEARIZATION

Input–output feedback linearization is applied in this section to devise robust sliding-mode controllers for the QSPRC. The main steps of the design procedure can be summarized as follows.

- The first step is to calculate the relative degree associated with the input–output linearization. The desired closed-loop output-voltage dynamics can then be specified according to the relative degree of $\bar{v}_o$.

- The choice of the sliding surface S constitutes the second step. Here, we introduce the use of the invariance condition to synthesize proper sliding functions that cancel part of the nonlinearities and guarantee the tracking convergence toward the particular output-voltage dynamics.

- The last step to get a satisfactory controller is to analyze the stability of the closed-loop system.

A. Relative Degree of $\bar{v}_o$

The relative degree of a state variable is the smallest number of differentiations of the variable with regards to time, so that the control input u appears explicitly [22]. From (10)–(16), it can be easily found that

$$\frac{\partial}{\partial u}\left(\frac{d^i \bar{v}_o}{dt^i}\right) = 0, \qquad \text{for } i = 1, 2, 3 \tag{17}$$

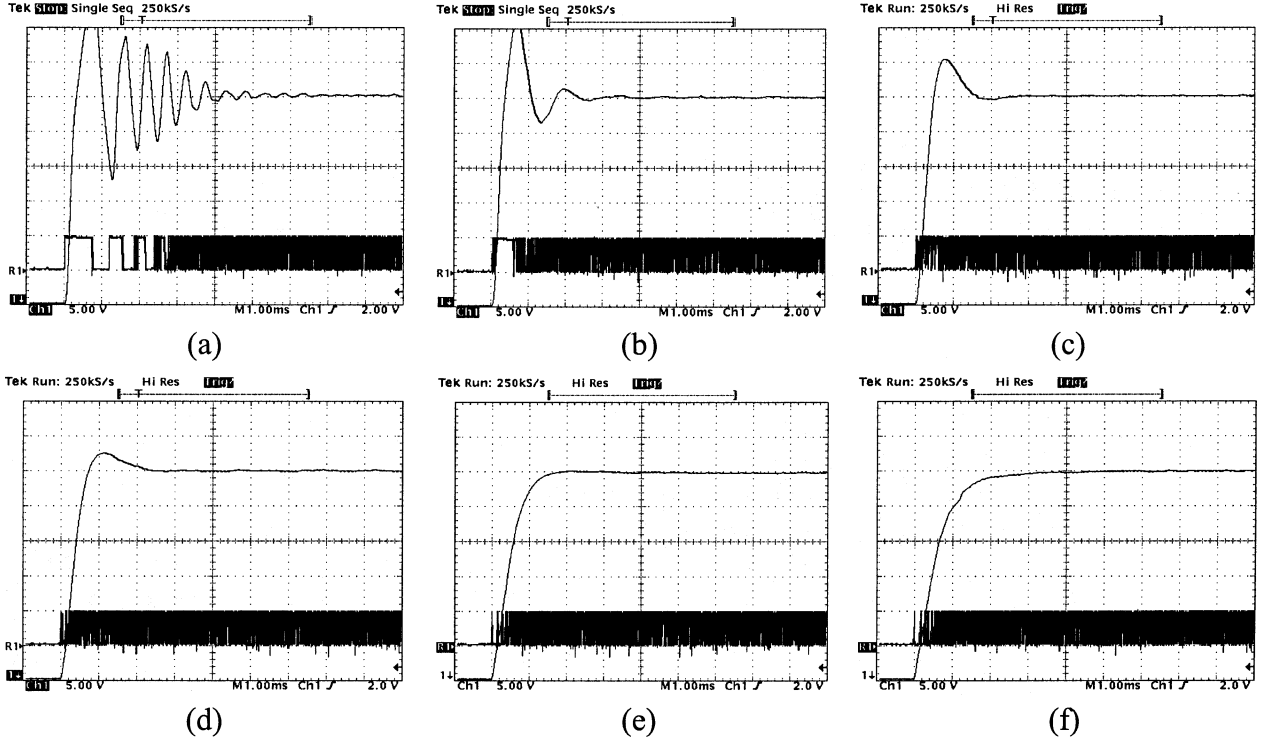$$\frac{\partial}{\partial u}\left(\frac{d^i \bar{v}_o}{dt^i}\right) \neq 0, \qquad \text{for } i = 4 \tag{18}$$

Fig. 9. Experimental startup of output voltage and control signal $u(kT)$ for different values of k_i: (a) 5120, (b) 470, (c) 190, (d) 120, (e) 60, and (f) 40. Top: output voltage (5 V/div). Bottom: control signal $u(kT)$ (10 V/div).

then, the relative degree of $\overline{v}_o$ is four. In that case, the open-loop output-voltage dynamics can be expressed as follows:

$$a_4 \cdot \frac{d^4 \overline{v}_o}{dt^4} + a_3 \cdot \frac{d^3 \overline{v}_o}{dt^3} + a_2 \cdot \frac{d^2 \overline{v}_o}{dt^2} - a_1 \cdot \frac{d^2 \overline{v}_{cp}}{dt^2} = 0 \quad (19)$$

with $a_4 = L_f C_{\mathrm{eq}} C_o$, $a_3 = L_f C_{\mathrm{eq}}/R$, $a_2 = C_{\mathrm{eq}}$, $a_1 = C_{\mathrm{eq}}/n$, and

$$\frac{d^2 \overline{v}_{cp}}{dt^2} = -\frac{1}{C_{\mathrm{eq}}} \cdot \left(\frac{\pi^2}{8} \cdot \left(\frac{Z_o \omega_o \overline{i}_f \cos \overline{\beta}}{n(1+A)\omega_r L_{\mathrm{eq}}} + \overline{i}_L \cdot \frac{d\overline{\beta}}{dt} \right) \right.$$
$$\left. \cdot \sin \overline{\beta} + \frac{1}{n} \cdot \frac{d\overline{i}_f}{dt} \right) + \left(\frac{\pi^2}{8} \cdot \frac{E \cos \overline{\beta}}{L_{\mathrm{eq}} C_{\mathrm{eq}}} \right) \cdot u. \quad (20)$$

The desired closed-loop output-voltage dynamics is a linear combination of the output-voltage time derivatives

$$b_4 \cdot \frac{d^4 \overline{v}_o}{dt^4} + b_3 \cdot \frac{d^3 \overline{v}_o}{dt^3} + b_2 \cdot \frac{d^2 \overline{v}_o}{dt^2} + b_1 \cdot \frac{d\overline{v}_o}{dt} + b_o \cdot (\overline{v}_o - V_{\mathrm{oref}}) = 0 \quad (21)$$

where the gains b_i cannot be zero, and the term $b_o \cdot V_{\mathrm{oref}}$ is included to get $\overline{v}_o = V_{\mathrm{oref}}$ in steady state. Notice that the order of the specified dynamics coincides with the relative degree of the output voltage; otherwise, the desired dynamics cannot be ensured by the control action.

B. Synthesis of Sliding Surfaces

In the sliding regime, the converter dynamics are forced to evolve over the sliding surface S, according to the invariance condition $\dot{S} = 0$ [22]. Such property can be used to design a control that guarantees the desired dynamics (21). In fact, by

subtracting (19) from (21) and equalizing the result to the invariance condition $\dot{S} = 0$, we obtain

$$\dot{S} = \sum_{i=2}^{4} (b_i - a_i) \cdot \frac{d^i \overline{v}_o}{dt^i} + b_1 \cdot \frac{d\overline{v}_o}{dt} + b_o \cdot (\overline{v}_o - V_{\mathrm{oref}}) + a_1 \cdot \frac{d^2 \overline{v}_{cp}}{dt^2} = 0 \quad (22)$$

and, consequently,

$$S = \sum_{i=2}^{4} (b_i - a_i) \cdot \frac{d^{i-1} \overline{v}_o}{dt^{i-1}} + b_1 \cdot \overline{v}_o + b_o \cdot \int (\overline{v}_o - V_{\mathrm{oref}}) d\tau + a_1 \cdot \frac{d\overline{v}_{cp}}{dt}. \quad (23)$$

The above surface satisfies transversal and existence conditions and also ensures absence of output-voltage steady-state errors due to the presence of the integral term [22]. Besides sensing only the voltages v_{cp} and v_o, the terms of surface (23) can be implemented using conventional low-cost electronic circuitry.

In addition, by choosing the coefficients b_i as follows: $b_4 = a_4$, $b_3 = a_3$, $b_2 = a_2 + k_d$, $b_1 = k_p$, and $b_o = k_i$, the surface (23) can be made even more simple

$$S = k_p \cdot \overline{v}_o + k_i \cdot \int (\overline{v}_o - V_{\mathrm{oref}}) d\tau + k_d \cdot \frac{d\overline{v}_o}{dt} + k_c \cdot \frac{d\overline{v}_{cp}}{dt} \quad (24)$$

with $k_c = a_1$. This simplification allows the designer to choose only the values for the parameters b_2, b_1, and b_o (the two remaining parameters b_4 and b_3 are fixed by the power-stage components). The loss of freedom in the assignment of values for the coefficients b_4 and b_3, however, does not present important restrictions to the imposition of the desired dynamics to $\overline{v}_o$, as we will see in Section V. In fact, a wide range of different transient
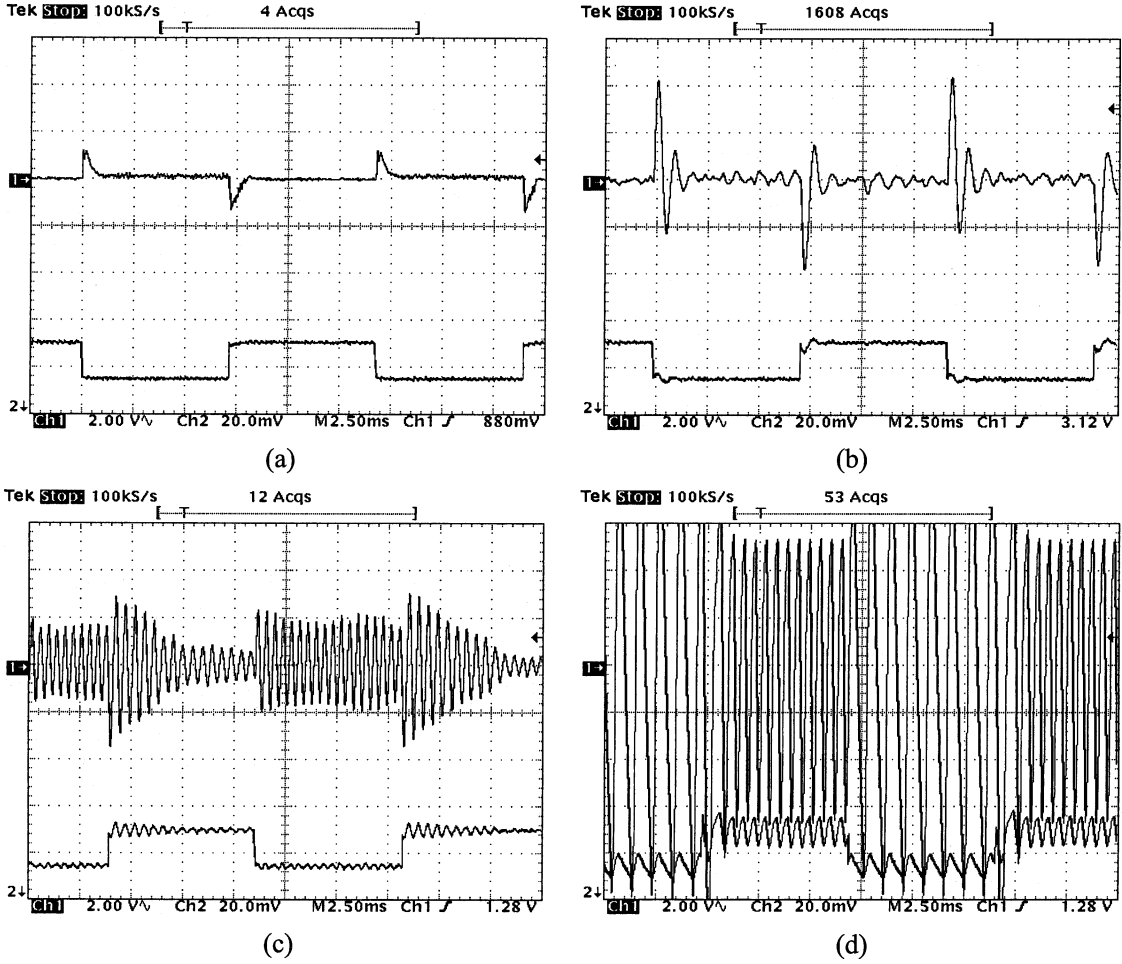
Fig. 10. Experimental transient response to load step changes. (a) Nominal control parameters. (b) $k_c = 0$. (c) $k_d = 0$. (d) $k_p = 0$. Top: output voltage (2 V/div). Bottom: load current (0.2 A/div).

responses (voltage overshoot, settling time) can be obtained, varying the values of the parameters b_2, b_1, and b_o. For these reasons, we choose the surface (24) to evaluate the validity of the design methodology described above.

The controller design ends up with the control law derivation. Applying the often-used reaching condition $S \cdot \dot{S} < 0$ [22], the control law can be expressed as

$$u = \begin{cases} 1, & \text{for } S < 0 \\ 0, & \text{for } S > 0. \end{cases} \qquad (25)$$

Fig. 4 shows a diagram of the sliding-mode controller using the sliding surface (24). Linear analog circuits can build the blocks that make up the sliding curve, and a comparator and a flip-flop constitute the control law, resulting in a simple and low-cost control loop, as predicted in the analysis.

C. Analysis of the System Stability

The closed-loop dynamics can be easily found by using the equivalent control concept [22]. Replacing the expression of this theoretical variable in the open-loop model (10)–(16) and

defining a new state variable by means of the nonlinear transformation $\bar{i}_{L_{eq}} = (\pi^2/8) \cdot \bar{i}_L \cdot \cos\overline{\beta}$, the ideal sliding dynamics results in

$$\frac{1}{n} \cdot \frac{d\bar{i}_{Leq}}{dt} = \left(\frac{1}{n^2} - \frac{k_d}{C_o}\right) \cdot \frac{d\bar{i}_f}{dt} - \left(k_p - \frac{k_d}{RC_o}\right) \cdot \frac{d\overline{v}_o}{dt}$$
$$- k_i \cdot (\overline{v}_o - V_{\text{oref}}) \qquad (26)$$

$$\frac{d\overline{v}_{cp}}{dt} = \frac{1}{C_{\text{eq}}} \cdot \left[\bar{i}_{Leq} - \frac{\bar{i}_f}{n}\right] \qquad (27)$$

$$\frac{d\bar{i}_f}{dt} = \frac{1}{L_f} \cdot \left[\frac{\overline{v}_{cp}}{n} - \overline{v}_o\right] \qquad (28)$$

$$\frac{d\overline{v}_o}{dt} = \frac{1}{C_o} \cdot \left[\bar{i}_f - \frac{\overline{v}_o}{R}\right] \qquad (29)$$

$$\frac{d\overline{v}_{cs}}{dt} = \frac{8AZ_o\omega_o}{\pi^2(1+A)} \cdot \frac{\bar{i}_{Leq} \cdot \cos\overline{\alpha}}{\cos\overline{\beta}} \qquad (30)$$

$$\frac{d\overline{\alpha}}{dt} = \omega_o \cdot \left[\frac{\omega_r}{\omega_o} - \frac{8AZ_o}{\pi^2(1+A)} \cdot \frac{\bar{i}_{Leq} \cdot \sin\overline{\alpha}}{\overline{v}_{cs} \cdot \cos\overline{\beta}}\right] \qquad (31)$$

$$\frac{d\overline{\beta}}{dt} = \omega_o \cdot \left[\frac{\omega_r}{\omega_o} - \frac{8Z_o}{\pi^2(1+A)} \cdot \frac{\bar{i}_{Leq} \cdot tg\overline{\beta}}{\overline{v}_{cp}}\right]. \qquad (32)$$

Notice that the dynamics of $\bar{i}_{Leq}$, $\overline{v}_{cp}$, $\bar{i}_f$, and $\overline{v}_o$ are linear, that is, the model (10)–(16) has been partly linearized by the design process (the number of exact linearized variables coincides with

the relative degree of $\overline{v}_o$). Moreover, these external dynamics are uncoupled to the internal variables ($\overline{v}_{cs}$, $\overline{\alpha}$, $\overline{\beta}$), so the stability of this subsystem can be tested using well-known linear techniques. In doing so, the following design restrictions can be deduced in terms of the converter components and the control parameters:

$$0 < k_p < \frac{C_{\text{eq}} + k_d}{R C_o} \tag{33}$$

$$k_d > - C_{\text{eq}} \tag{34}$$

$$0 < k_i < \frac{R^2 C_o k_p}{L_f C_{\text{eq}}} \cdot \left(\frac{C_{\text{eq}} + k_d}{R C_o} - k_p \right). \tag{35}$$

On the other hand, a simple way of demonstrating the stability of the internal dynamics expressed in (30)–(32) is using the zero-dynamics approach [20]. The zero dynamics are defined as the internal dynamics of the system when the output is kept at its equilibrium value and, then, all of its time derivatives are zero. By means of small-signal linearization, it can be easily found that the zero dynamics of (30)–(32) present local asymptotic stability. Moreover, the zero dynamics are independent of the control parameters, so no design conditions are derived from this analysis.

Fig. 5 shows the stability region in the $k_p - k_i$ plane, using the nominal values listed in Table II. Fixing $k_p = 0.042 \ \Omega^{-1}$, the minimum and maximum values of k_i for stable operation are 0 and 36144, respectively. For this range of k_i, the loci of the external dynamics eigenvalues are depicted in Fig. 6.

Finally, Fig. 7 shows some simulation results of the closed-loop QSPRC during the output-voltage startup for different values of k_i. Notice that a wide range of transient responses is obtained varying the gain of only one sliding surface parameter (the coefficient b_o of the desired output-voltage dynamics).

V. EXPERIMENTAL RESULTS

A high-frequency QSPRC prototype with the sliding-mode controller diagrammed in Fig. 4 was built and tested. The nominal values of the power-stage components and control parameters are listed in Table II.

Fig. 8 shows the output-voltage startup of the prototype for the same values of k_i used in the simulations (see Fig. 7). Only slight differences can be observed when comparing these simulation and experimental results. However, when control enters into the saturation region (high values of k_i gain), the transient responses are not exactly linear as expected. Fig. 9 depicts some examples of such saturation events.

Fig. 10 shows the transient responses of the output voltage and the load current when the resistive load is abruptly changed. Four different situations were considered. First, nominal control parameters were used, showing good transient and steady-state characteristics. The next experiments eliminate some terms of the sliding surface (with the remaining gains unchanged), proving that all terms are necessary. Although not shown in figures, a slightly better behavior was obtained in the second ($k_c = 0$) and third cases ($k_d = 0$) modifying appropriately the surface gain parameters. In the last case ($k_p = 0$), however, no improvements were observed when changing the surface gains.

In fact, this situation corresponds to an unstable behavior, as predicted in (33).

VI. CONCLUSION

In this paper, we have addressed the problem of designing proper sliding-mode control schemes to regulate the output voltage of the QSPRC. First, we established an averaged large-signal model, which constitutes the appropriate description of the power circuit for control design purposes. Second, a promising control design approach based on input–output feedback linearization was proposed. The application of the design procedure to the averaged model leads to a family of sliding surfaces that make the output voltage of the QSPRC behave following a desired large-signal linear dynamics. Among these surfaces, the final configuration was selected taking into account a simple and low-cost practical implementation. The features of the proposed control solution include linear output-voltage transient responses, absence of steady-state output-voltage errors, and robust operation with respect to parameter variation and external disturbances (both in the voltage source and in the load).

Finally, a set of design restrictions arising from the stability analysis was established. Such conditions were expressed in terms of the power circuit components and the parameters of the desired output-voltage dynamics, thus facilitating the subsequent design procedure. The validity of the theoretical predictions has been confirmed by means of simulations and experimental results.

REFERENCES

[1] P. R. Chetty, "Resonant power supplies: Their history and status," *IEEE Aerosp. Electron. Syst. Mag.*, vol. 7, no. 4, pp. 23–29, Apr. 1992.

[2] R. Oruganti and F. C. Lee, "Resonant power processors, Part II—Methods of control," *IEEE Trans. Ind. Appl.*, vol. 21, no. 6, pp. 1461–1471, Nov./Dec. 1985.

[3] M. G. Kim and M. J. Youn, "An energy feedback control of series resonant converters," *IEEE Trans. Power Electron.*, vol. 6, no. 4, pp. 338–345, Jul. 1991.

[4] J. M. Carrasco, E. Galván, G. E. Valderrama, R. Ortega, and A. Stankovic, "Analysis and experimentation of nonlinear adaptative controllers for the series resonant converter," *IEEE Trans. Power Electron.*, vol. 15, no. 3, pp. 536–544, May 2000.

[5] G. B. Joung, C. T. Rim, and G. H. Cho, "An integral cycle mode control of series resonant converter," in *Proc. IEEE PESC'88*, 1988, pp. 575–582.

[6] G. B. Joung and G. H. Cho, "Modeling of quantum parallel resonant converters controlled by integral cycle mode," in *Proc. IEEE PESC'89*, 1989, pp. 744–751.

[7] W. H. Kwon and G. H. Cho, "Optimum quantum sequence control of quantum series resonant converter for minimum output voltage ripple," *IEEE Trans. Power Electron.*, vol. 9, no. 1, pp. 74–84, Jan. 1994.

[8] J. H. Ko, S. S. Hong, M. G. Kim, and M. J. Youn, "Modeling and improved current control of series resonant converter with nonperiodic integral cycle mode," *IEEE Trans. Power Electron.*, vol. 7, no. 2, pp. 280–288, Apr. 1992.

[9] F. Boudjema and J. L. Abatut, "Sliding mode. A new way to control series resonant converters," in *Proc. IEEE IECON'90*, 1990, pp. 938–943.

[10] P. Bidan, M. Valentin, and L. Martinez, "Modeling and current-mode control of a zero-current switching resonant converter used for AC-sine voltage generation," in *Proc. IEEE PESC'93*, 1993, pp. 636–640.

[11] B. R. Jo, H. W. Ahn, G. W. Moon, H. C. Choi, and M. J. Youn, "Decoupled output voltage control of quantum series resonant converter for improved Buck-Boost operation," *IEEE Trans. Power Electron.*, vol. 11, no. 1, pp. 146–161, Jan. 1996.

[12] M. Castilla, L. García de Vicuña, M. López, O. López, and J. Matas, "On the design of sliding mode control schemes for quantum resonant converters," *IEEE Trans. Power Electron.*, vol. 15, no. 6, pp. 960–973, Nov. 2000.

[13] M. Castilla, L. García de Vicuña, M. López, and V. Barcons, "An averaged large-signal modeling method for resonant converters," in *Proc. IEEE IECON'97*, 1997, pp. 447–452.

[14] S. R. Sanders, J. Noworolski, X. Liu, and G. C. Verghese, "Generalized averaging method for power conversion systems," *IEEE Trans. Power Electron.*, vol. 6, no. 5, pp. 251–259, Sep. 1991.

[15] E. X. Yang, F. C. Lee, and M. M. Jovanovic, "Extended describing function technique applied to the modeling of resonant converters," in *Proc. VPEC PES*, 1991, pp. 179–191.

[16] H. Sira-Ramirez and M. Ilic, "Exact linearization in switch mode dc-to-dc power converters," *Int. J. Control*, vol. 50, pp. 511–524, Aug. 1989.

[17] H. Sira-Ramirez, "Switched control of bilinear converters via pseudo-linearization," *IEEE Trans. Circuits Syst.*, vol. 36, no. 6, pp. 858–865, Jun. 1989.

[18] H. Sira-Ramirez and M. Rios-Bolívar, "Sliding mode control of dc-to-dc power converters via extended linearization," *IEEE Trans. Circuits Syst. I, Fundam. Theory Appl.*, vol. 41, no. 10, pp. 652–661, Oct. 1994.

[19] O. López, "Imposición de dinámica en los sistemas electrónicos de potencia. Una nueva perspectiva en el diseño de controladores," Ph.D. dissertation, Dept. Electron. Eng., Univ. Politécnica Cataluña, Vilanova í la Geltrú, Spain, 2000.

[20] J. J. Slotine and W. Li, *Applied Nonlinear Control*. Englewood Cliffs, NJ: Prentice-Hall, 1991.

[21] M. Kazimierczuk, N. Thirunarayan, and S. Wang, "Analysis of series-parallel resonant converter," *IEEE Trans. Aerosp. Electron. Syst.*, vol. 29, no. 1, pp. 88–99, Jan. 1993.

[22] J. Y. Hung, W. Gao, and J. C. Hung, "Variable structure control: A survey," *IEEE Trans. Ind. Electron.*, vol. 40, no. 1, pp. 2–22, Feb. 1993.

Luis García de Vicuña received the Ingeniero de Telecomunicación and Dr.Ing. Telecomunicación degrees from the Universidad Politécnica de Cataluña, Barcelona, Spain, in 1980 and 1990, respectively, and the Dr.Sci. degree from the Université Paul Sabatier, Toulouse, France, in 1992.

From 1980 to 1982, he was an Engineer with the Control Applications Company. He is currently an Associate Professor in the Departamento de Ingeniería Electrónica, Universidad Politécnica de Cataluña, where he teaches power electronics. His research interests include power electronics modeling, simulation and control, active power filtering, and high-power-factor ac/dc conversion.

Josep María Guerrero received the B.S. degree in telecommunication engineering, the M.S. degree in electronic engineering, and the Ph.D. degree from the Universidad Politécnica de Cataluña, Barcelona, Spain, in 1997, 2000, and 2003, respectively.

Since 1998, he has been an Assistant Professor in the Department of Automatic Control Systems and Computer Engineering, Universidad Politécnica de Cataluña, where he teaches control theory and microprocessors. His research interests include DSP-based control, uninterruptible power supplies, and distributed power systems.

José Matas received the B.S., M.S., and Ph.D. degrees in telecommunications engineering from the Universidad Politécnica de Cataluña, Barcelona, Spain, in 1988, 1996, and 2003, respectively.

Since 1997, he has been an Assistant Professor in the Departamento de Ingeniería Electrónica, Universidad Politécnica de Cataluña. His research interests include power-factor-correction circuits, distributed power systems, and nonlinear control.

Miguel Castilla received the M.S. and Ph.D. degrees in telecommunications engineering from the Universidad Politécnica de Cataluña, Barcelona, Spain, in 1995 and 1998, respectively.

Since 2002, he has been an Associate Professor in the Departamento de Ingeniería Electrónica, Universidad Politécnica de Cataluña, where he teaches analog circuits and power electronics. His research interests are in the areas of modeling, simulation, and control of dc-to-dc power converters and high-power-factor rectifiers.

Jaume Miret (M'98) received the B.S. (Telecommunications) and M.S. (Electronics) degrees in 1992 and 1999, respectively, from the Universidad Politécnica de Cataluña, Barcelona, Spain, where he is currently working toward the Ph.D. degree in the Departamento de Ingeniería Electrónica.

Since 1993, he has been an Assistant Professor at the Universidad Politécnica de Cataluña. His research interests include dc-to-ac converters, active power filters, and digital control.